J Mater Sci: Mater Electron
DOI 10.1007/s10854-008-9590-8

Capacitance and resistance measurements of SnO_2 thick-films

Miguel Adolfo Ponce · Miriam S. Castro · Celso M. Aldao

Received: 27 November 2007 / Accepted: 14 January 2008

Abstract Impedance spectroscopy measurements on SnO_2 thick films were carried out in an air atmosphere and for temperatures between 25 and 425 °C. Capacitance and resistance analyses reveal the mechanisms responsible for experimental responses. Four different contributions to the overall capacitance and resistance were distinguished and assigned to the bulk, the grain boundary, the electrodes, and the presence of deep traps. The effects of trap states on the electrical behavior of the sensor were explored and a modified equivalent circuit model is proposed.

1 Introduction

Chemical sensors based on tin oxide present a high sensitivity under atmosphere variations but they have a poor selectivity and a low thermal stability. The electrical properties of SnO_2 gas sensors depend on the oxide non-stoichiometry, on the incorporated additives, on the ceramic powders preparation method, and on the temperature and atmosphere during thermal treatments. Different methods are used for the synthesis of doped and undoped powders of SnO_2: sol–gel, oxalates and hydroxides precipitation, polymeric precursors, solid state reactions through the carbonates decomposition, vapor phases deposition, and SnO oxidation to SnO_2 through epitaxial growth [1–3]. It is well known that the Pechini's method permits to obtain nanoparticles that have been successfully used to make electrical devices [4]. For the employed powders, different factors (such as type of defects, morphology, and additives) contribute to the electrical response of the gas sensor [5, 6].

The film conductance is broadly used to characterize a sensor. Less attention has been paid to the electrical capacitance. However, adsorption of gaseous species at the grain boundaries can induce changes in the barriers heights and in the donor concentration [7]. These changes can be followed through measurements of capacitance using impedance spectroscopy [8].

In this work, tin oxide nanoparticles were printed onto insulating alumina substrates with Au nonporous electrodes. Thick films were made with the screen printed method. Later, impedance spectroscopy measurements on resulting SnO_2 thick films, in an air atmosphere at different temperatures, were carried out. A sequential analysis of the film capacitance and resistance as a function of frequency is presented. Finally, an equivalent electrical circuit is proposed to model the electrical behavior of the SnO_2 film.

2 Experimental

2.1 Powder preparation

In this work, the Pechini's method was used to obtain nanoparticles. Analytical grades of $SnCl_2 \cdot 2H_2O$ (Baker) were employed as a tin source. In a previous work, we have successfully obtained tin oxide gas sensors using this method. Pechini's method details are reported in reference [9]. X-ray powder diffraction analyses were carried out with a Philips PW 1830/40 equipment running with CoKα radiation.

M. A. Ponce (✉) · M. S. Castro · C. M. Aldao
Institute of Materials Science and Technology (INTEMA), University of Mar del Plata and National Research Council (CONICET), Juan B. Justo 4302, B7608FDQ Mar del Plata, Argentina
e-mail: mponce@fi.mdp.edu.ar

2.2 Sample preparation

Using the screen-printing technique [9], thick film samples were made mixing the powders with glycerol in a 2:1 ratio, and painting with the obtained paste onto insulating alumina substrate on which gold electrodes with an interdigited shape had been deposited by sputtering. Finally, in order to improve the mechanical adhesion and to avoid the grain growth, samples were thermally treated in an oven for 2 h, in air, at 500 °C. The mean thickness of the films was ~100 μm, as measured using a coordinates measuring machine Mitutoyo BH506. A Jeol JSM-6460 LV microscope under the secondary electrons mode (SE) was employed to image the tin oxide surfaces.

2.3 Measurement setup

Wide-frequency-range electrical measurements were performed on a variety of impedance analyzers with overlapping ranges. The measurement frequency range was from 10^{-2} to 15 MHz. First, the electrical behavior of the tin oxide films was analyzed using impedance plots in which the impedance Z is shown in a complex plane with the reactance, the imaginary part Z'', plotted against the resistance, the real part Z' [10, 11]. The system was linked to a computer for programming the measurements and for storing and handling the data. Z'' versus Z' curves were obtained at different temperatures in a dry air atmosphere (760 mmHg). The impedance data have been measured in the temperature range between 25 and 425 °C. The increasing, and then decreasing, rate was ~1 °C/min. When a measure temperature was reached, and previous to the data acquisition, to ensure that the system is in steady state, the temperature was kept constant until measurements did not vary with time. Three different temperatures were selected for data analysis: 100, 250 and 425 °C. Finally, the electrical resistance and capacitance were determined and fitted with an R(RC) equivalent circuit using the software Zview 2.1. A sequential number of measurements were carried out for each temperature and the relative error was lower than 3%.

3 Results and discussion

From the XRD analysis only the presence of SnO_2 was detected. With the scanning electron microscopy (SEM) technique, a highly porous microstructure with nanoparticles of 150 nm was observed.

In Fig. 1 we present impedance plots corresponding to three temperatures. In this type of plot, the impedance is shown in a complex plane with the reactance plotted against the resistance. Impedance plots reflect the bulk resistance (R_b), and grain boundary resistance (R_{gb}) and capacitance (C_{gb}) [12]. Results can be fitted with a simple $R_b(R_{gb}C_{gb})$ electrical model [8, 12]. The impedance of a resistance R_{gb} in parallel with a capacitance C_{gb} is given by

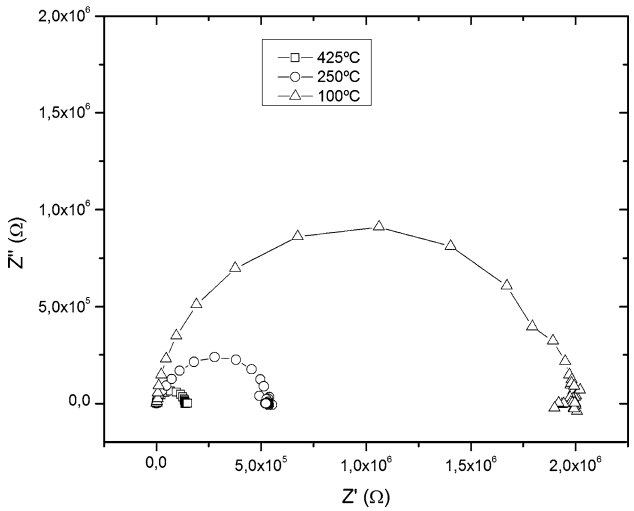

Fig. 1 Impedance plots corresponding to three temperatures. Z is shown in a complex plane with the reactance, the imaginary part Z'', plotted against the resistance, the real part Z'

$$Z_{gb} = \frac{R_{gb}\frac{1}{j\omega C_{gb}}}{R_{gb} + \frac{1}{j\omega C_{gb}}}, \tag{1}$$

where $\omega = 2\pi f$. Equation 1 can be expressed as

$$\left(Z'_{gb} - R_{gb}/2\right)^2 + Z''^2_{gb} = \left(R_{gb}/2\right)^2, \tag{2}$$

where Z'_{gb} and Z''_{gb} are the real and imaginary components of Z_{gb}, respectively. The corresponding plot of the real against imaginary part of Z_{gb} is a circumference of radius $R_{gb}/2$ centered at $R_{gb}/2$. The addition of a series resistance R_b only shifts the resulting circle. Thus, R_{gb} and R_b are derived from the low- and high-frequency resistance values, respectively, and the capacity can be found from the maximum value of the reactance. It can be observed that the radius of the resulting semi-circles become smaller with increasing temperature. This indicates that grain boundary resistance decreases with temperature, effect that is expected since current transport mechanisms are all thermally facilitated.

Very frequently, for a better analysis of the impedance measurements, the imaginary component of complex capacitance as $C''(\omega) = Z'/(\omega(Z'^2 + Z''^2))$ and the real component of the capacitance as $C'(\omega) = Z''/(\omega(Z'^2 + Z''^2))$ are calculated [13]. We propose here an alternative study in which the total parallel equivalent capacitance (C_p) and the total parallel resistance (R_p) as a function of frequency are analyzed.

In Figs. 2 and 3, the electrical resistance and capacitance of a SnO_2 thick film are plotted as a function of frequency at 425 °C. The observed behaviors cannot be reproduced with a simple RC circuit indicating that a more sophisticated electrical circuit model needs to be considered [14]. Indeed, a more complex circuit has been proposed in which the effect of bulk and electrode is incorporated as seen in Fig. 4 [15–17]. In the circuit of Fig. 4, three different contributions to the overall impedance were postulated: grain boundary, bulk, and electrode contact. Figure 2 shows that the resistance remains constant up to ~100 kHz and then rapidly decreases. With the circuit proposed in Fig. 4, the R_p frequency dependence can be reproduced. On the other hand, Fig. 3 shows that the capacitance remains almost constant at high frequencies. Conversely, at low frequencies (<1 kHz) a clear dependence of the capacitance with frequency is observed. This result cannot be reproduced with the circuit presented in Fig. 4.

Now we will focus on the C_p response at frequencies lower than 100 Hz (see Fig. 3). Even assuming a quite high value for the electrode capacitance (10^{-5} F), the C_p frequency response cannot be reproduced [18, 19]. It is found that the electrode contact can only be responsible for a rapid quadratic decrease around 10–200 Hz. Figure 3 shows that for frequencies lower than 1 Hz, the C_p fitting remains constant around 0.5 nF. Also, a $1/f^2$ dependence of the C_p fitting with frequency is observed in Fig. 3, while the experimental values show a $1/f$ dependence at frequencies lower than 100 Hz. We conclude that the C_p low frequency response cannot be explained with the only presence of an electrode contact.

We propose that the film electrical behavior at low frequencies can be better described with the electrical model shown in Fig. 5a, where, for the sake of simplicity, R_b is neglected. In this circuit, the resistance R_t and the capacitance C_t mimic the effect of deep traps [14]. The total conductivity (G_p) and total capacitance (C_p) for this circuit can be expressed as follows:

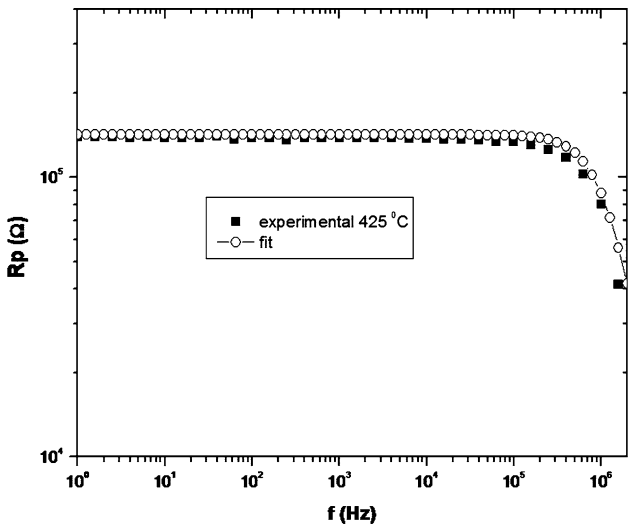

Fig. 2 Resistance as a function of frequency at 425 °C. Empty symbols correspond to simulation fittings (using the equivalent circuit of Fig. 4) and filled symbols to the experimental results. For the fitting, the R_{gb} value is determined from experimental results of Fig. 1(at low frequencies). For 425 °C the R_{gb} value is 1.4×10^5 Ω. The C_{gb} is determined from the experimental results showed in Fig. 3 at high frequencies. For 425 °C the C_{gb} value is 7×10^{-12} F. The R_e and the C_e employed were obtained from previously reported results in polycrystalline semiconductors ($\sim C_e = 10^{-5}$ F and $R_e = 1$ kΩ) [10, 18, 19]. The C_b can be considered negligible ($C_b \sim 10^{-14}$) and the R_b value (1.5 kΩ) was estimated from the corner frequency (20 kHz) in Fig. 2

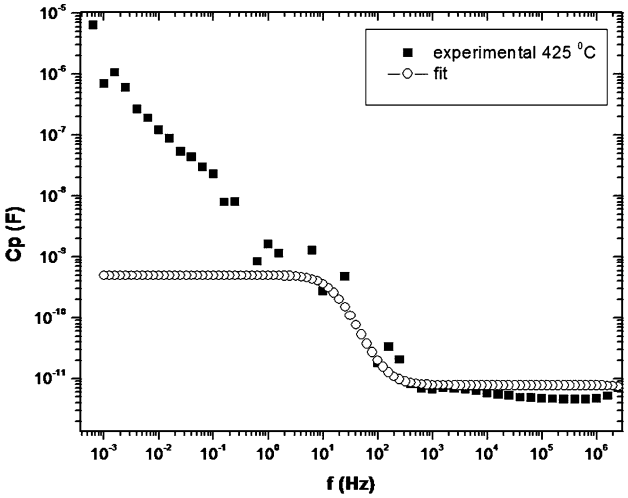

Fig. 3 Capacitance as a function of frequency at 425 °C. Empty symbols correspond to simulation fittings (using the equivalent circuit of Fig. 4) and filled symbols to the experimental results. $C_{gb} = 7 \times 10^{-12}$ F, $R_{gb} = 1.4 \times 10^5$ Ω, $C_b = 5 \times 10^{-14}$ F, $R_e = 1$ kΩ, $R_b = 1.5$ kΩ, and even assuming a quite high value for the electrode capacitance (10^{-5} F, [10, 18, 19]), C_p cannot be reproduced

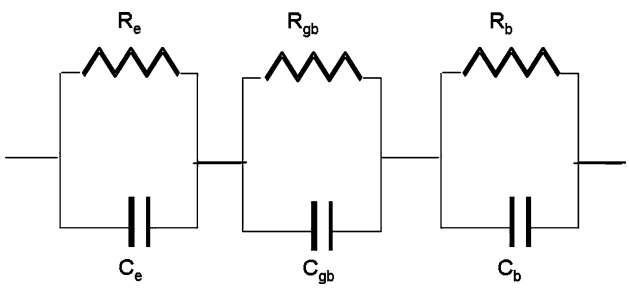

Fig. 4 Equivalent circuit that includes three different contributions to the overall impedance: grain boundary, bulk, and electrode contact. R_{gb} and C_{gb} represent the grain boundary resistance and capacitance, respectively. R_b and C_b represent the bulk resistance and capacitance, respectively. The electrode elements are R_e and C_e

$$G_p = \frac{1}{R_{gb}} + C_t\omega^2 \frac{\tau}{1+\omega^2\tau^2} \tag{3}$$

and

$$C_p = C_{gb} + C_t \frac{1}{1+\omega^2\tau^2}, \tag{4}$$

where, $\tau = C_t R_t$ is the mean lifetime of the traps.

Based on the model of Fig. 5a, R_{gb} and C_{gb} can be determined from the conductance and capacitance values in the limits of very low and very high frequencies, respectively, i.e.

$$G_{tot}|_{\omega\to 0} = \frac{1}{R_{gb}} \tag{5}$$

and

$$C_{tot}|_{\omega\to\infty} = C_{gb}. \tag{6}$$

Here, C_{gb} was measured at frequencies above 10 kHz and R_{gb} between 1 and 10^{-2} Hz.

In Fig. 6a and b we present plots for C_{tot} and G_{tot} resulting from the circuit of Fig. 5a. C_{tot} and R_{tot} show inflection points that correspond to certain critical frequencies, usually named "corner frequencies". Analytical values of the corner frequencies for C_{tot} can be found to be:

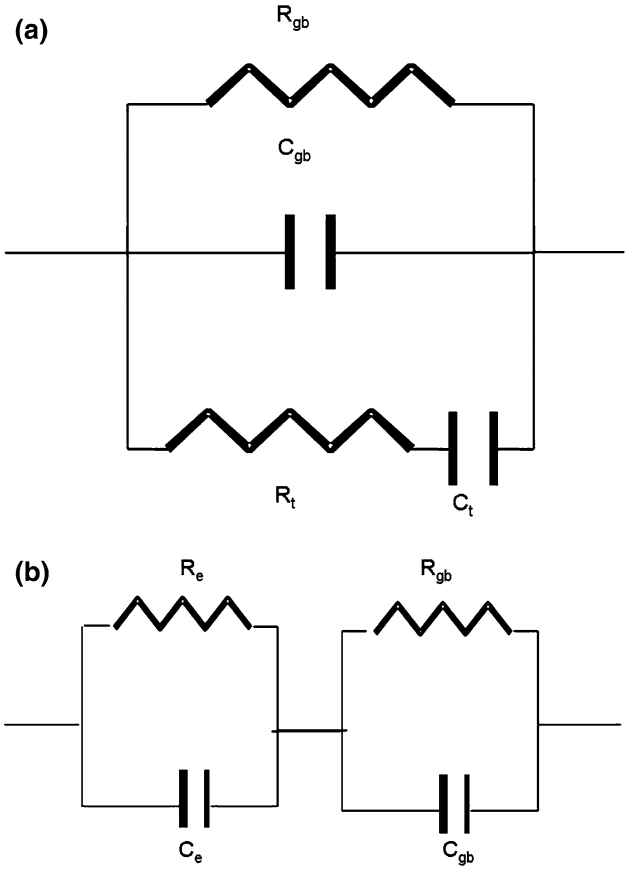

Fig. 5 (**a**) Model introducing deep bulk trap contributions. R_t and C_t represent the effect of deep traps. (**b**) Circuit with the same overall impedance at all frequencies that the circuit of (**a**)

$$\omega_1 = \frac{1}{R_t C_t}, \tag{7}$$

$$\omega_2^2 = \frac{1}{C_t C_{gb} R_t^2}. \tag{8}$$

From the model of Fig. 5a, the capacitance values at low (<100 Hz) and high frequencies (>1 kHz) correspond to the addition of C_t and C_{gb} and to C_{gb}, respectively, as shown in Fig. 6a.

Analytical values of the corner frequencies for R_{tot} can be expressed as follows:

$$\omega_a^2 = \frac{1}{R_t R_{gb} C_t^2}, \tag{9}$$

and

$$\omega_b = \frac{1}{R_t C_t}. \tag{10}$$

Also, the values of R_{tot} corresponding to very low (<100 Hz) and very high (>1 kHz) frequencies are R_{gb} and

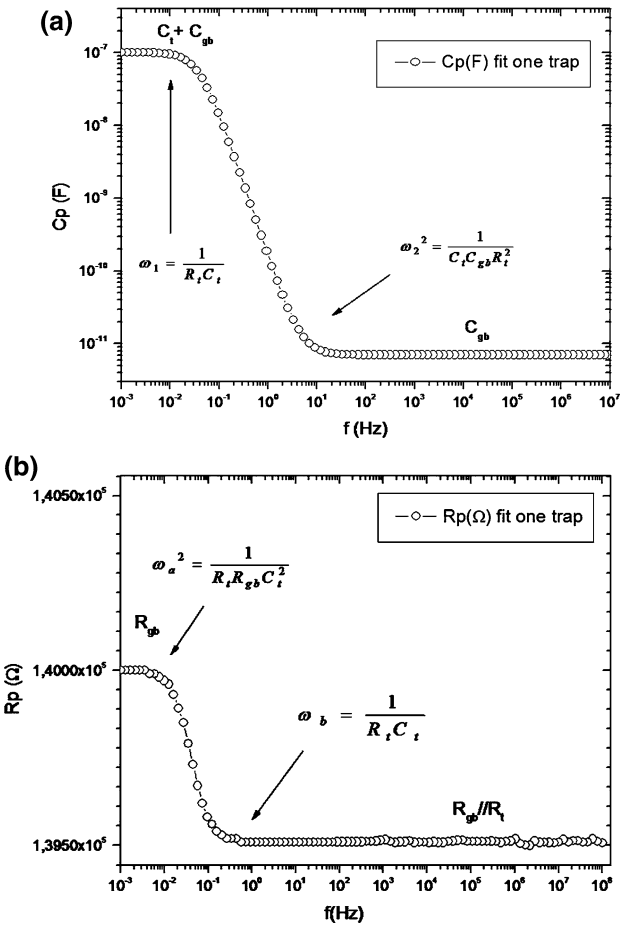

Fig. 6 C_p (**a**) and R_p (**b**) as a function of frequency resulting from the circuit 5a. Different inflection points that correspond to certain critical frequencies, usually named "corner frequencies", are shown. The resistance and capacitance values employed are: $R_{gb} = 1.4 \times 10^5\ \Omega$, $C_{gb} = 7 \times 10^{-12}$ F, $R_t = 4 \times \Omega$ and $C_t = 10^{-7}$ F

the parallel of R_{gb} and R_t. At frequencies around 10^{-2} Hz, R_{tot} shows a small decrease due to R_{gb} and R_t component elements that are in parallel (see Fig. 6b).

We must note that, the circuits of Fig. 5a and b can present the same overall impedance at all frequencies when their elements are properly interrelated. This means that these circuits are equivalent for specific values of their elements; choosing between these circuits must involve other type of considerations rather than frequency response. Indeed, one may use some knowledge on the processes involved and compare the circuits with the predictions of physical models.

We will summarize next the relations between the elements of the two circuit elements shown in Fig. 5. From Fig. 5a elements to Fig. 5b elements, the relations can be expressed as follows.

$$C_{gb(a)} = \frac{C_{gb(b)}C_e}{C_{gb(b)} + C_e} \tag{11}$$

$$C_t = \frac{(R_{gb(b)}C_{gb(b)} - R_eC_e)^2}{(C_{gb(b)} + C_e)(R_{gb(b)} + R_e)^2} \tag{12}$$

$$R_{gb(a)} = R_{gb(b)} + R_e \tag{13}$$

$$R_t = \frac{R_{gb(b)}R_e(R_{gb(b)} + R_e)(C_e + C_{gb(b)})^2}{(R_{gb(b)}C_{gb(b)} + R_eC_e)^2}, \tag{14}$$

where the subscripts a and b correspond to the circuit element of Fig. 5a and b, respectively. Given the orders of magnitude of the circuit elements for our case, Eqs. 11–14 can be simplified to

$$C_{gb(a)} = C_{gb(b)} \tag{15}$$

$$C_t = \frac{C_eR_e^2}{R_{gb(b)}^2} \tag{16}$$

$$R_{gb(a)} = R_{gb(b)} \tag{17}$$

$$R_t = \frac{R_{gb(b)}^2}{R_e}. \tag{18}$$

To reproduce the frequency response of Fig. 3 with the circuit of Fig. 5b, the value of C_e should be around 10^{-2} F which is a non physical value for the electrode capacitance. This indicates that the circuit of Fig. 5b is not appropriated to describe the experiments.

Experimental data (capacitance and resistance for T = 425 °C) were fitted with an RC in parallel with an RC series equivalent circuit using the Zview 2.1 program for Windows. The R_{gb} value (140 kΩ), which corresponds to the R_{tot} value measured at low frequencies, was obtained from Fig. 2. The value of C_{gb} (7×10^{-12} F) was determined from Fig. 3 at high frequency. Then, R_t and C_t can be readily estimated from the R_{tot} and C_{tot} values at low and high frequencies, respectively. Also, R_t and C_t can be determined from ω_2 and ω_b. In a first approach, with only one trap, the estimated values were 4.5×10^{-9} F for C_t and 22 MΩ for R_t, respectively. In Fig. 7, empty symbols correspond to a simulation of the experimental results (filled symbols) at 425 °C. Empty circles correspond to a simulation with one trap and empty triangles to a simulation with two traps. Certainly, better fittings to experiments can be obtained when a large number of different traps as RC series are added in parallel (see Fig. 7). The capacitance dependence with frequency suggests an even more complex circuit. We considered the possibility of multi-traps as described with the circuit of Fig. 8a.

The disordered deep bulk trap location in SnO_2 grains could be the phenomenon that modifies the Debye-like response. The usual circuit element used to model the Debye deviations is the Constant Phase Element (CPE) as shown in the circuit of Fig 8b. Although we usually use ideal resistors, capacitances, and inductances in an equivalent circuit, actual real elements only approximate ideality over a limited frequency range. When dealing not with a single activation energy but with a distribution of activation energies, one passes from a simple ideal resistor and capacitor in parallel or series to a distributed impedance element. A constant phase element (CPE) is a simple distributed element that produces an impedance having a constant phase angle in the complex plane [20].

A CPE is an empirical impedance function of the following form

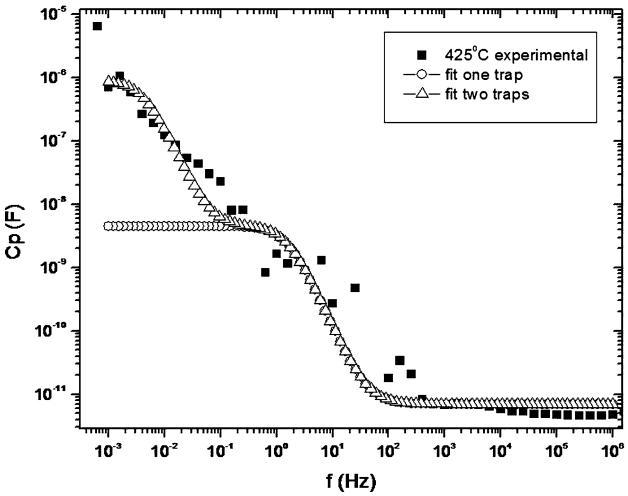

Fig. 7 Capacitances as a function of frequencies at 425 °C. Empty symbols correspond to simulation fittings (using the equivalent circuit of Fig. 5a) and filled symbols to the experimental results. Empty circles correspond to a simulation with one trap and empty triangles to a simulation with two traps (n = 2 in Fig. 8a). The elements values are: $C_{gb} = 7 \times 10^{-12}$ F, $R_{gb} = 1.4 \times 10^5$ Ω, $C_{t(1)} = 4.5 \times 10^{-9}$ F, $R_{t(1)} = 2.2 \times 10^7$ Ω, $C_{t(2)} = 9 \times 10^{-7}$ F, $R_{t(2)} = 4 \times 10^7$ Ω

$$Z_{CPE} = \frac{1}{A(j\omega)^{\alpha}}. \tag{19}$$

The constant A determines the impedance modulus and the exponent α determines the impedance angle. In the special case of $\alpha = 1$, the CPE acts like a capacitor with A equal to the capacitance. The CPE can also behave as an inductance, $\alpha = -1$, or a resistance, $\alpha = 0$. A CPE is regularly used in a model in place of a capacitor to compensate for non-homogeneities in the system [20]. At low frequencies, the equivalent capacitance of the circuit of Fig. 8b is given by

$$C_p = C_{gb} + \frac{A.sen(\alpha\pi/2)}{\omega^{1-\alpha}}, \tag{20}$$

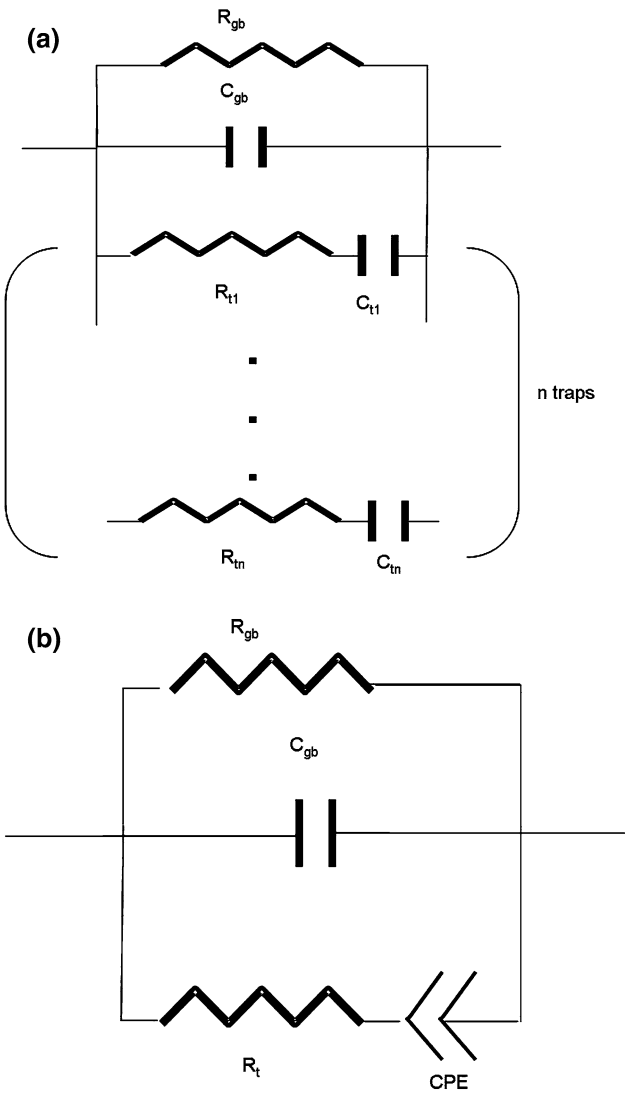

Fig. 8 (**a**) Equivalent circuit with multi-traps. (**b**) The proposed circuit to model the Debye deviations. A Constant Phase Element (CPE) is incorporated

that shows a slope that depends on the parameter α. With the circuit of Fig. 8b, the capacitance low frequency response can be reasonably reproduced as seen in Fig. 9.

Finally, despite the fitting enhancement achieved with the CPE, the electrode and bulk presence cannot be eluded. A final model, including the electrode and bulk effects, is shown in Fig. 10. To corroborate the above considerations, new fittings were carried out with the proposed model of Fig. 10. In Fig. 11 the fittings of the C_p response with frequency is shown. Another step to improve the equivalent circuit consists in the inclusion of a grain size distribution. This would reflect as a distribution in the grain boundary and bulk equivalent circuit elements values (R_{gb}, R_b, C_{gb} and C_b values).

To conclude, and gain confidence on the proposed model of Fig. 10, fittings for 100 and 250 °C were carried out. The values of the circuit elements obtained from these

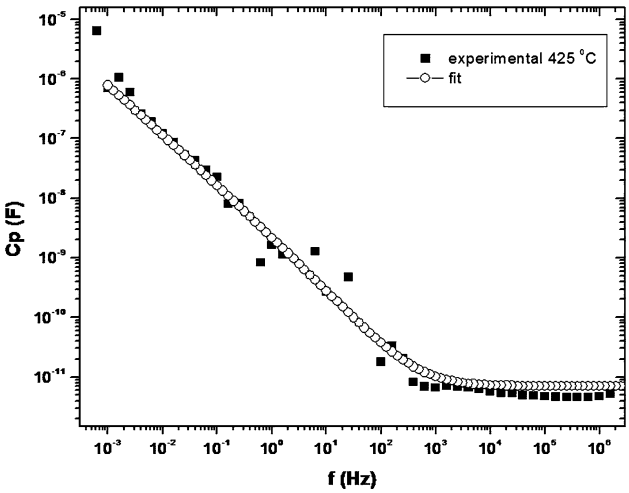

Fig. 9 Capacitance as a function of frequency at 425 °C. Empty symbols correspond to simulation fittings (using the equivalent circuit of Fig. 8b) and filled symbols to the experimental results. The resistances and capacitances values employed were $C_{gb} = 7 \times 10^{-12}$ F, $R_{gb} = 1.4 \times 10^5\ \Omega$, $CPE_{(1-a)} = 0.2$, $CPE_{(A)} = 5 \times 10^{-8}$ and $R_t = 4 \times 10^6\ \Omega$

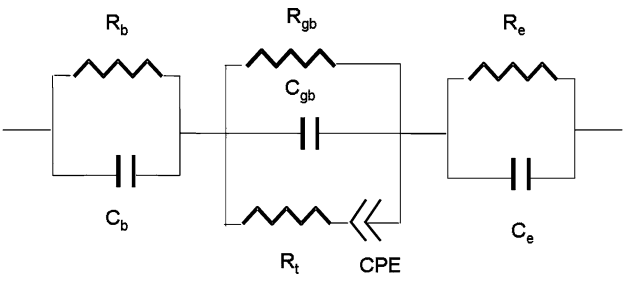

Fig. 10 Final proposed model considering the electrode, grain boundary, traps, and bulk equivalent elements. Deep bulk traps are represented with the incorporation of a R_t element in series with a *CPE*

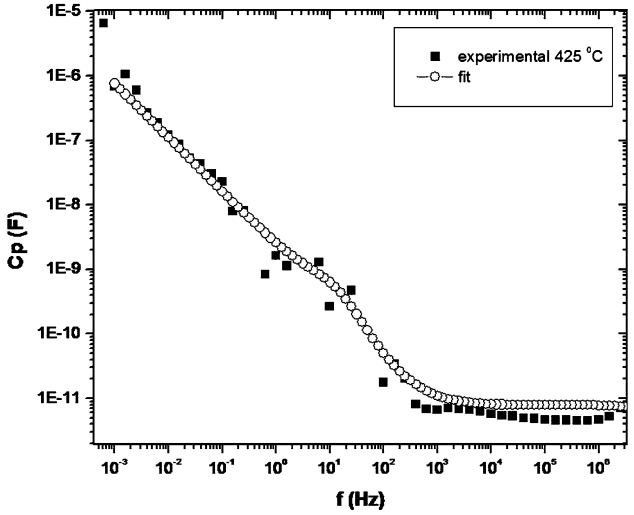

Fig. 11 Capacitance fitting plots as a function of frequency at 425 °C in air atmosphere considering the electrical equivalent circuit proposed in Fig. 10. The employed elements values were $C_{gb} = 7 \times 10^{-12}$ F, $R_{gb} = 1.4 \times 10^5$ Ω, $CPE_{(1-a)} = 0.2$, $CPE_{(A)} = 5 \times 10^{-8}$, $R_t = 4 \times 10^6$ Ω, $C_e = 1 \times 10^{-5}$ F, $R_e = 1{,}000$ Ω, $C_b = 5 \times 10^{-14}$ F and $R_b = 1{,}500$ Ω

Table 1 Components values obtained from the fittings, for 100, 250 and 425 °C

Element	100 °C	250 °C	425 °C
R_{gb} (Ω)	2×10^6	5.3×10^5	1.4×10^5
C_{gb} (F)	4×10^{-12}	5×10^{-12}	7×10^{-12}
R_t (Ω)	7×10^7	5×10^7	4×10^6
$CPE_{(A)}$	5×10^{-8}	5×10^{-8}	5×10^{-8}
CPE $(1 - \alpha)$	0.2	0.2	0.2
R_e (Ω)	1,200	1,100	1,000
C_e (F)	1×10^{-5}	1×10^{-5}	1×10^{-5}
R_b (Ω)	1,700	1,600	1,500
C_b (F)	5×10^{-14}	5×10^{-14}	5×10^{-14}

fittings, and for 425 °C, are shown in Table 1. In particular, note that the elements from the equivalent circuit of Fig. 5a (R_{gb}, C_{gb}, R_t and CPE elements) are the main responsible for the C_p and R_p responses with frequency at different temperatures. Using the proposed model, the obtained values of the equivalent circuit elements R_{gb}, C_{gb}, R_t and CPE are in the same order of magnitude of previous results (16). Finally, a deeper analysis could be carried out considering different atmospheres and gas concentration. The resistance R_{gb} decreases with temperature, effect that is expected since current transport mechanisms are all facilitated with temperature [21–23]. Conversely, the grain boundary capacitance (C_{gb}) is not very affected by temperature in this range. These results are consistent with previously reported results in polycrystalline semiconductors [10]. On the other hand, notorious changes of R_t values are detected as temperature facilitates the activation of more and more traps.

4 Conclusions

Usually the electrical behavior of tin oxide thick films is modeled with an (RC) parallel equivalent circuit. However, experiments show impedance frequency responses that this simple circuit cannot reproduce; a more sophisticated model needs to be considered. We showed that the frequency dependence of the total resistance can be assigned to the bulk contribution and that the frequency dependence of the total capacitance to the presence of deep bulk traps. More specifically, expected deep traps, with a distribution of activation energies, imply a distributed impedance element. Finally, the electrode effects are also incorporated. With the proposed model, the temperature influence on resistance and capacitance can be fitted and is consistent with the suggested interpretation.

Acknowledgements The authors express their thanks to CONICET and the University of Mar del Plata for the financial support, to Jorge Rodríguez Páez and Alejandra Montenegro (University of Cauca, Colombia) for the powders preparation and to Hector Ascencio for the technical support.

References

1. J.C. Giuntini, W. Granier, J.V. Zanchetta, A. Taha, J. Mater. Sci. Lett. **9**, 1383 (1990)
2. E.R. Leite, J.W. Gomes, M.M. Oliveira, E.J.H. Lee, E. Longo, J.A. Varela, C.A. Paskocimas, T.M. Baaoschi, F. Lanciotti, P.S. Pizani, P.C. Soares, J. Nanosci. Nanotechnnol. **2**, 125 (2002)
3. A. Prodan, N. Vene, F. Sevsek, M. Hudomal, Thin Solid Films **147**, 313 (1987)
4. A.C. Bose, P. Balaya, P Thangadurai, S. Ramasamy, J. Phys. Chem. Solids **64**, 659 (2003)
5. S. Capone, P. Siciliano, F. Quaranta, R. Rella, N. Epifani, L. Vasanelli, Sensor Actuat. B Chem. **3911**, 1 (2001)
6. C. Xu, J. Tawaki, N. Miura, N. Yamazoe, Sensor Actuat. B Chem. **3**, 147 (1991)
7. M. Labeau, U. Schmatz, G. Delabouglise, J. Roman, M. Valalet-Regi, A. Gaskow, Sensor Actuat. B Chem. **26**, 49 (1995)
8. M.A. Ponce, M.S. Castro, C.M. Aldao, Mater. Sci. Eng. B **111**, 14 (2004)
9. A. Montenegro, M. Ponce, M.S. Castro, J.E. Rodríguez-Paez, J. Eur. Ceram. Soc. **27**, 4143 (2007)
10. S. Saukko, V. Lantto, Thin Solid Films **436**, 137 (2003)
11. R.H Cole, K.S. Cole, J. Chem Phys. **9**, 341 (1941), ibid., **10**, 98 (1942)
12. M. Seitz, F. Hampton, W. Richmond, in *Advanced in Ceramics*, vol. 7, ed. by M.F. Yan, A.H. Heuer (The American Ceramic Society Inc., Ohio, 1983), pp. 60–70
13. G. Garcia-Belmonte, J. Bisquert, F. Fabregat-Santiago, Solid State Electron. **43**, 2123 (1999)
14. B.S. Chiou, M.C. Chung, J. Electron. Mater. **20**, 885 (1991)

15. N. Barsan, D. Koziej, U. Weimar, Sensor Actuat. B Chem. **121**, 18 (2007)
16. U. Weimar, W. Gopel, Sensor Actuat. B Chem. **26–27**, 13 (1995)
17. T.P. Hulser, H. Wiggers, F.E. Kruis, A. Lorke, Sensor Actuat. B Chem. **109**, 13 (2005)
18. A.K. Jonscher, J.-M. Réau, J. Mater. Sci. **13**, 553 (1978)
19. J.T.S. Irvine, D.C. Sinclair, Adv. Mater. **2**, 132 (1990)
20. J. Ross Macdonald, *Impedance Spectroscopy, Emphasizing Solid Materials and Systems* (John Wiley & Sons Inc. Publications, Canada, 1987)
21. M.S. Castro, C.M. Aldao, Appl. Phys. Lett. **63**, 1077 (1993)
22. M.S. Castro, C.M. Aldao, J. Eur. Ceram. Soc. **17**, 1533 (1997)
23. M.A. Ponce, C.M. Aldao, M.S. Castro, J. Eur. Ceram. Soc. **23**, 2105 (2003)